

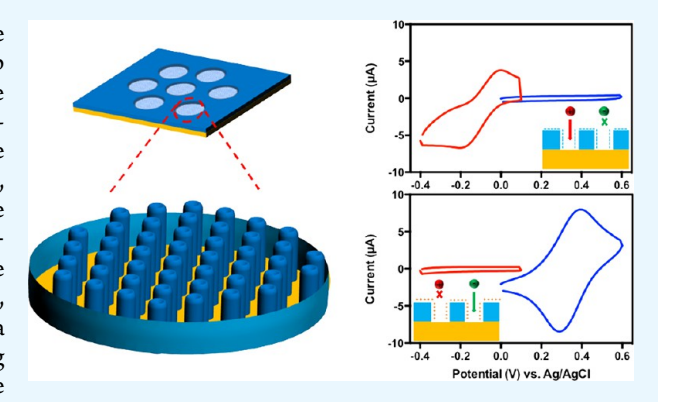
Nanochannel Arrays for Molecular Sieving and Electrochemical Analysis by Nanosphere Lithography Templated Graphoepitaxy of **Block Copolymers**

Kaiyu Fu[†] and Paul W. Bohn*,†,‡

†Department of Chemistry and Biochemistry and [‡]Department of Chemical and Biomolecular Engineering, University of Notre Dame, Notre Dame, Indiana 46556, United States

Supporting Information

ABSTRACT: The ability to design, fabricate, and manipulate materials at the nanoscale is fundamental to the quest to develop technologies to assemble nanometer-scale pieces into larger-scale components and materials, thereby transferring unique nanometer-scale properties to macroscopic objects. In this work, we describe a new approach to the fabrication of highly ordered, ultrahigh density nanochannel arrays that employs nanosphere lithography to template the graphoepitaxy of polystyrenepolydimethylsiloxane, diblock copolymers. By optimizing the well-controlled solvent vapor annealing, overcoating conditions, and the subsequent reactive ion etching processes, silica nanochannel (SNC) arrays with areal densities, ρ_A , approaching 1000 elements μm^{-2} , are obtained over macroscopic scales. The integrity and functionality of the SNC arrays was tested by using



them as permselective ion barriers to nanopore-confined disk electrodes. The nanochannels allow cations to pass to the disk electrode but reject anions, as demonstrated by cyclic voltammetry. This ion gating behavior can be reversed from cationpermselective to anion-permselective by chemically inverting the surface charge from negative to positive. Furthermore, the conformal SNC array structures obtained could easily be lifted, detached, and transferred to another substrate, preserving the hierarchical organization while transferring the nanostructure-derived properties to a different substrate. These results demonstrate how nanoscale behavior can be replicated over macroscale distances, using electrochemical analysis as a model.

KEYWORDS: nanosphere lithography, graphoepitaxy, block copolymers, nanochannel arrays, ion accumulation, electrical double-layer effect, permselectivity

1. INTRODUCTION

There is substantial interest in developing large-scale structures from nanoscale components in such a way that the nanoscalederived behavior is retained. Such a capability would not only open up new practical applications but also lead to improved fundamental understanding of the differences between the physicochemical properties of nanosystems and those of larger structures. 1-3 One interesting example involves macroscale arrays of nanopore-confined electrodes capable of capturing mass-limited samples and investigating their electrochemical behavior in zeptoliter-volume nanopores. 4-6 Such nanopore electrodes can mimic the function of biological nanopores and can also transform biorecognition events into robust electrical signals at high temporal resolution.^{7,8} Compared to single nanopore electrodes, nanopore electrode arrays (NEAs) exhibit nanoscale properties, e.g., strongly interacting electric double layers⁹⁻¹¹ and surface-charge-dominated transport, ¹²⁻¹⁴ but they produce much larger currents because the current signal is integrated over many parallel nanopores. 15,16 Recently, we have reported size- and charge-mediated current signals, resulting from the unique mass transport and ion accumulation properties of these structures. 17,18 In order to optimally utilize this combination of properties, it would be useful to fabricate spatially uniform NEAs with high areal density over macroscopic scales.

Early examples of NEAs with ultrasmall nanopatterns (down to 20 nm) were typically fabricated by electron beam lithography (EBL)^{19–21} and focused ion beam (FIB) milling, 22,23 but these serial direct-write approaches are restricted by time and cost to fabrication of high density patterns over limited (µm-scale) areas. In contrast to these top-down approaches, bottom-up approaches provide an alternative way to fabricate nanostructures with comparable precision and are amenable to highly parallel fabrication of nanostructures at the wafer scale. 24,25 The self-assembly of block copolymers (BCPs) is a convenient way to fabricate highly ordered arrays with

Received: May 14, 2017 Accepted: June 29, 2017 Published: June 29, 2017 tunable nanostructure, including spheres, cylinders, lamellae, etc.^{26,27} By selectively removing one block through chemical etching or physical processing, the remaining block can preserve the original hierarchical nanostructures.²⁸ While spontaneous self-assembly results in randomly oriented microscale domains with substantial defect densities, chemical 29,30 and topographical patterns^{31–34} or external fields^{35,36} are typically used to trigger BCP self-assembly into well-ordered hierarchical nanostructures. Additionally, in most cases BCPs tend to form in-plane—rather than vertical—nanocylinders, especially when the two blocks have a distinctly different surface energy or large γ values. Thus, fabricating vertically aligned nanochannels, as desired in NEAs for electroanalysis, presents another challenge. Two principal approaches have been used: (1) indirect alignment through anisotropic dry etching of a nanoporous template over a sacrificial underlayer³⁷⁻³⁹ and (2) in situ formation of high aspect (pore depthto-diameter) vertical nanochannels.^{40–42} The first approach is limited because most polymers show low resistance to dry etching. Even using silicon-doped polymers, high aspect ratio nanopores are difficult to achieve. The challenge in the second approach is to form sub-20 nm vertical nanodomains, which require a large Flory-Huggins parameter (χ) and small molecular weight, on a large scale. Thus, in most cases, BCPs tend to form in-plane, rather than vertical, nanocylinders, especially when the two blocks have distinctly different surface energies or large γ values. Recently, new approaches involving surface neutralization 40,43 or top coating 44,45 have been used to address these challenges and form vertical nanocylinders over relatively large scales. Both strategies rely on the surface modification to minimize the large difference in surface energy of two distinct blocks of BCPs.

In this work, we develop a novel approach to the preparation of highly ordered, vertically oriented nanopore arrays on a large scale by using nanosphere lithography (NSL) to template the graphoepitaxy of polystyrene/polydimethylsiloxane, PS-b-PDMS, BCPs. Using polystyrene beads, an NSL-patterned substrate with micrometer-scale corrals is obtained that provides spatial confinement and directs the self-assembly of BCPs with long-range lateral order. By using well-controlled solvent vapor annealing and top coating processes, we obtain nanostructures with areal densities, ρ_A approaching 1000 elements μm^{-2} over macroscopic distances. Silica nanochannel (SNC) arrays are produced from these by selective O₂ plasma to remove the PS block and convert the PDMS block of the BCPs into silica. The combination of NSL templating, graphoepitaxy, vertical alignment, and O2 processing represents a new route to the production of highly aligned, ultrahigh density nanocylinders capable of functioning as high-sensitivity permselective NEAs. These resulting SNC arrays exhibit strong electrochemical polarity due to the permselective nature of the nanochannels. For example, they selectively allow cations access to the bottom disk electrode while at the same time rejecting anions. The polarity of this ion gating property can be reversed through a one-step surface chemical modification, which inverts the SNC array surface charge from negative to positive. The resulting structures can be removed from the original substrate by lift-off and transferred to another substrate for subsequent use, further enhancing their utility for electrochemical analysis and other applications.

2. EXPERIMENTAL SECTION

2.1. Chemicals and Materials. Poly(styrene-*b*-dimethylsiloxane) (PS-b-PDMS, $M_w \sim 31.0$ -b-14.5 kg/mol, PDI ~ 1.09) was purchased from Polymer Source. 40% hydrolyzed poly(vinyl alcohol) (PVA-40, $M_{\rm w} \sim 72$ kg/mol) was purchased from Polysciences. 80% hydrolyzed poly(vinyl alcohol) (PVA-80, $M_{\rm w} \sim 9-10$ kg/mol), poly(methyl methacrylate) (PMMA, $M_{\rm w} \sim 350$ kg/mol), and polystyrene latex beads were obtained from Sigma-Aldrich. Hexaammineruthenium(III) chloride ([Ru(NH₃)₆]Cl₃), potassium hexacyanoruthenate(II) hydrate (K₄Ru(CN)₆), potassium hexacyanoferrate(III) (K₃Fe(CN)₆), potassium chloride (KCl), and hydrochloric acid (HCl) were also obtained from Sigma-Aldrich. All chemicals and organic solvents were used as received unless otherwise noted. ITO-coated glass slides (ITO thickness ~100 nm, $R_{\rm s}$ = 70–100 Ω) were obtained from Delta Technologies. Deionized (DI) water (18 MΩ·cm) purified using a Millipore Milli-Q system was used to prepare all aqueous solutions for electrochemical measurements.

2.2. Fabrication: NSL Templating. Precleaned ITO glass slides were prepared by sonicating in acetone for 10 min and subsequently rinsing consecutively with acetone, methanol, and DI water. Then SiO₂ circular corrals were defined on a precleaned ITO glass slide by nanosphere lithography. 46 In short, a 100 nm SiO₂ layer was deposited onto the precleaned ITO glass slide by chemical vapor deposition (Unaxis 790 Series, PECVD). Then the substrate was exposed to a short O₂ plasma to render the surface hydrophilic. After surface treatment, a self-assembled monolayer of polystyrene beads was transferred to the ITO glass slide by emersion through an air-water interface containing the beads. Then the polystyrene beads were reduced in size by O2 plasma etching, after which a thin layer of chromium was deposited by e-beam evaporation (Oerlikon 450B). Afterward, the polystyrene beads were removed by sonication in chloroform or acetone, thus producing the circular patterned Cr mask for subsequent SiO₂ etching (Plasma-Therm 790 RIE). It took ~2.5 min to etch 100 nm SiO₂ with an approximate etching rate of 40 nm/ min. Finally, the highly ordered SiO₂ circular trenches were achieved by wet etching to remove the Cr mask.

2.3. Fabrication: Graphoepitaxy. An amount of 1-5 wt % PS-b-PDMS solution in toluene was spin-coated at 6000 rpm onto precleaned or SiO₂-patterned ITO glass slides for 30 s, leading to a thickness of 40-200 nm. After drying in vacuum for 30 min, PS-b-PDMS films were spin coated with 2 wt % PVA solution, either PVA-40 in methanol or PVA-80 in DI water, at 6000 rpm for the 30 s. The whole substrate was dried under vacuum for another 30 min. The annealing process was performed either in the open on a hot plate at 150 °C for 2 h (thermal annealing) or inside a closed glass chamber with saturated solvent vapor for 2 h (solvent annealing). The solventannealed PS-b-PDMS films were quickly removed from the chamber to induce fast solvent evaporation. After annealing, the substrate was rinsed with methanol or DI water to remove the top PVA-40 or PVA-80 layer, respectively. In order to obtain the silica nanochannel (SNC) array, reactive ion etching was used to selectively etch the PS domain and simultaneously oxidize the PDMS to silica. Samples were exposed for 10 s to CF₄ (150 W, 50 sccm) and subsequently for 60 s to O₂ (90

PMMA-assisted transfer of the resulting SNC arrays followed the method of Su et al.⁴⁷ Briefly, 3 wt % PMMA/toluene solution was spin-coated on the SNC to form a thin protective layer on the top of the substrate. Subsequently, the whole substrate was immersed in 2 M HCl solution overnight to etch the entire underlying ITO layer and release the SNC/PMMA film from the substrate. Then, another hydrophilic ITO glass substrate was used to capture the SNC/PMMA film, after which it was heated at 100 °C for 2 h to strengthen the bonding between the SNC array and the ITO glass slide. Finally, the top PMMA layer was dissolved by placing the substrate in acetone for 3 h.

2.4. Characterization. Scanning electron microscopy (SEM) images were taken on an FEI-Helios Dual Beam FIB at an accelerating voltage of 5 kV. Prior to SEM imaging, all samples were sputter-coated with 2.5 nm iridium to avoid surface charging. Cyclic voltammetry

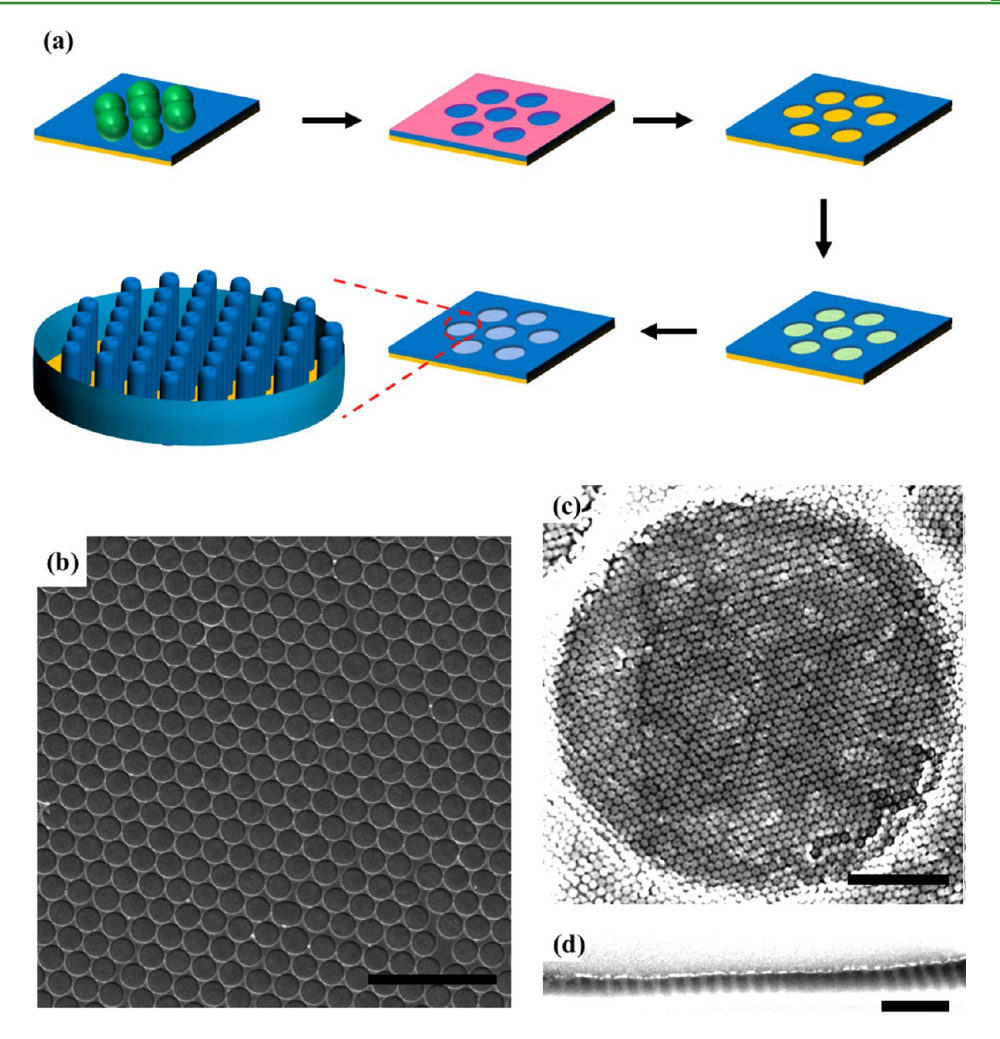


Figure 1. (a) Schematic illustration of NSL-templated graphoepitaxy of block copolymers used to fabricate NEAs. Colors indicate PS colloids (green), ITO glass slide (yellow), SiO_2 layer (blue), Cr layer (pink), and PS-b-PDMS (light green). (b) SEM image of highly ordered circular SiO_2 corrals fabricated by nanosphere lithography. Scale bar: $10 \ \mu m$. (c) Plan-view and (d) cross-sectional SEM images of ultrahigh density SNC arrays inside a single NSL-defined trench after O_2 plasma etching. Scale bars: upper 500 nm and bottom 200 nm.

(CV) experiments were performed on a CHI bipotentiostat (CH Instruments, model 842C). The ITO film was operated as the working electrode. Pt wire and Ag/AgCl were used as counter and reference electrodes, respectively. All potentials were reported vs Ag/AgCl at 300 K unless otherwise noted. During the electrochemical measurements, the Pt wire and Ag/AgCl counter and reference electrodes were immersed in a 200 μ L solution inside a 6 mm diameter PDMS reservoir. In all CV measurements, the potential of the ITO electrodes was scanned at 100 mV/s.

3. RESULTS AND DISCUSSION

3.1. Fabrication of SNC Arrays. As illustrated in Figure 1(a), consecutive application of nanosphere lithography (NSL) followed by graphoepitaxy and self-assembly of BCPs can be used to produce close-packed silica nanochannel (SNC) arrays at large scale. Under the proper conditions, the NSL-templated graphoepitaxially defined BCPs are sufficiently well-ordered to fabricate nanopore electrode arrays. Polystyrene (PS) beads with typical sizes from 300 nm to 5 μ m were chosen to template the formation of highly ordered separated circular patterns. These were obtained, rather than triangular nanocylinders, because O_2 plasma etching was used to controllably reduce the PS bead diameter by \sim 10–40% after which a protective Cr layer was applied by thermal evaporation. As

shown in Figure 1(b), well-defined circular SiO₂ corrals were obtained after releasing the PS beads, dry etching the underlying exposed SiO₂ layer to a predefined depth, and wet etching to remove the top Cr layer. Once the pattern of shallow SiO₂ corrals was defined, PS-b-PDMS ($M_{\rm w} \sim 31.0\text{-}b\text{-}14.5 \text{ kg/mol}$, PDI ~ 1.09) solution was spin-coated on the prepatterned substrate. Then a thin film of poly(vinyl alcohol) (PVA) was spin-coated over the top, and the entire structure was solvent vapor annealed to induce formation of vertical PDMS nanocylinders in PS.

PS- \dot{b} -PDMS was selected for this NSL-templated hierarchical fabrication method for two reasons. First, this BCP possesses a large Flory—Huggins interaction parameter ($\chi=0.26$), meaning that it can support strong phase separation, even for sub-10 nm features. In addition, the excellent etch selectivity between PS and PDMS blocks means that a short O_2 etch selectively removes PS and, at the same time, converts PDMS into silica nanocylinders. Figures 1(c) and 1(d) show plan-view and cross-sectional SEM images of the highly ordered SNC array obtained by confinement of the PS-b-PDMS in the NSL-templated SiO₂ circular corrals. The diameter and center-to-center distance of the silica nanocylinders in this sample were 29 and 36 nm, respectively, leading to an areal density (assuming perfect hcp packing) of $\rho_A \sim 890$ elements μm^{-2} . As

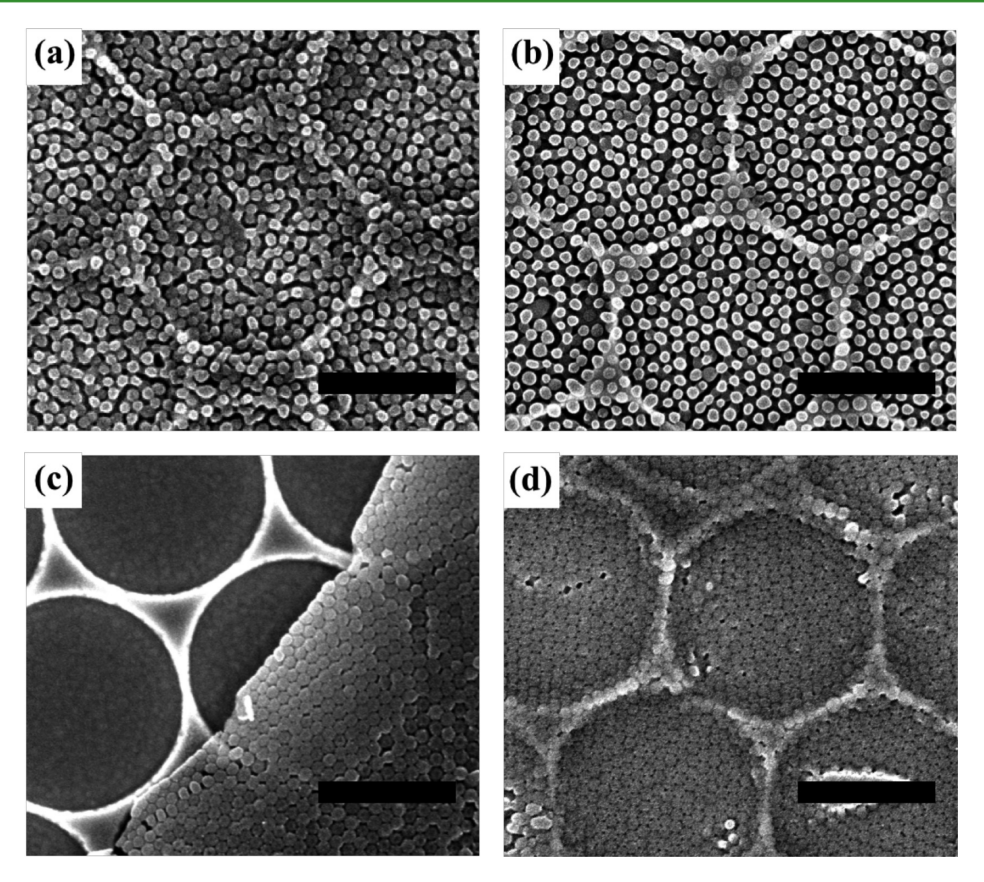


Figure 2. SEM images of PS-b-PDMS films inside circular SiO $_2$ corrals subjected to different processing conditions and subsequent reactive ion etching. (a) As-prepared PS-b-PDMS film. (b) PS-b-PDMS film with an overlayer of PVA-80 and thermal annealing. (c) PS-b-PDMS film with an overlayer of PVA-80 and acetone vapor annealing. All scale bars: 500 nm.

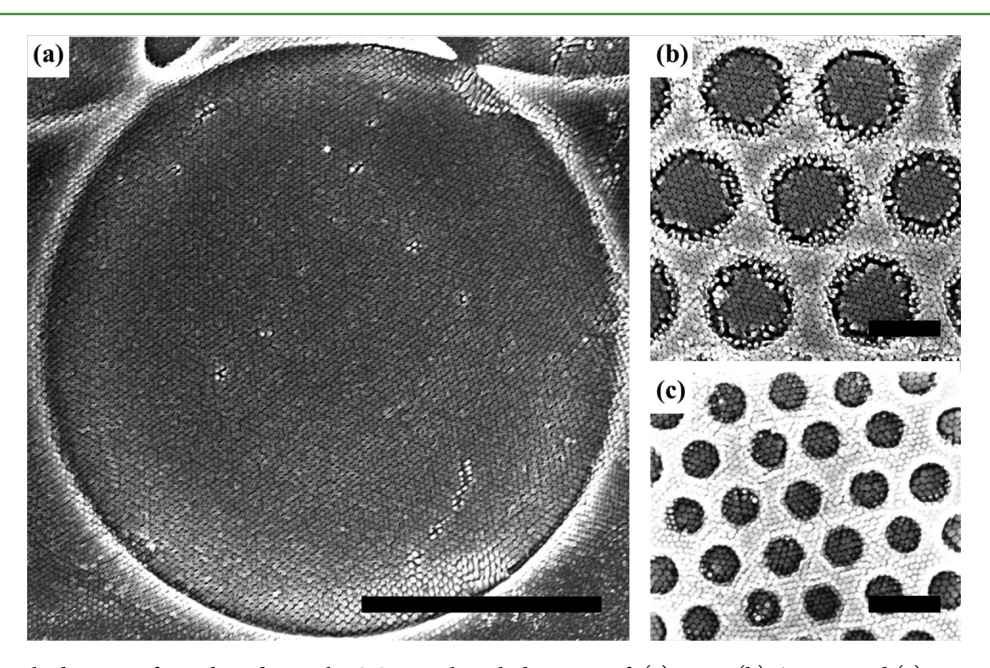


Figure 3. Silica nanocylinder arrays formed inside circular SiO_2 corrals with diameters of: (a) 5 μ m, (b) 600 nm, and (c) 250 nm. Scale bars: 2 μ m, 500 nm, and 500 nm, respectively.

shown in Figure 1(d), the length of the resulting silica nanocylinders was pinned to the depth of the SiO_2 corral, ca. 100 nm, by accurately controlling polymer concentration and spinning speed. The importance of confinement in producing highly ordered arrays is illustrated by comparison to nano-

cylinders formed from an unconfined cylindrical PS-b-PDMS phase. As shown in the plan-view and cross-sectional SEM images (Figure S1, Supporting Information), the PDMS-derived silica nanocylinders obtained under these conditions lack long-range order in the plane.

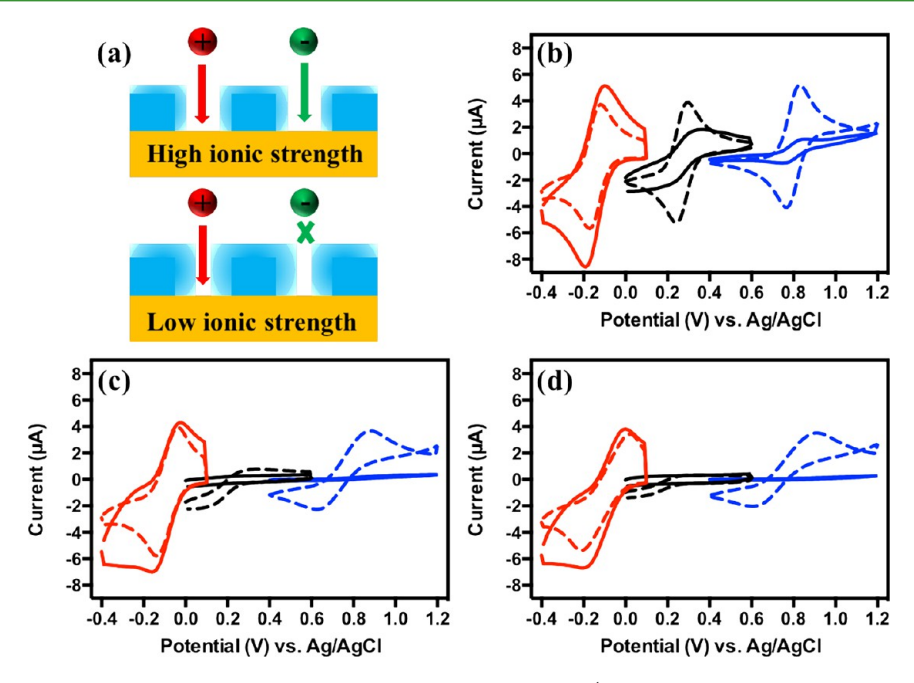


Figure 4. (a) Schematic illustration of permselective ion accumulation inside micropore (top, $\kappa d \gg 1$, where $\kappa =$ inverse Debye length and d = pore diameter) and nanopore (bottom, $\kappa d \sim 1$) electrode arrays. Cyclic voltammetry at a macroscopic (6 mm diam.) ITO electrode in KCl containing different redox species before (dashed line) and after (solid line) introduction of an SNC onto the ITO to produce an NEA. Voltammetry of 100 μM Ru(NH₃)₆³⁺ (red), Fe(CN)₆^{3−} (black), and Ru(CN)₆^{4−} (blue) in (b) 0.5 M KCl, (c) 1 mM KCl, and (d) 1 μM KCl.

Because of the large difference in surface energy between PS and PDMS ($\gamma_{PS} = 40.7 \text{ mN m}^{-1}$; $\gamma_{PDMS} = 20.4 \text{ mN m}^{-1}$), PS-b-PDMS with PDMS volume fraction, $f_{\rm PDMS} \sim 0.31$, tends to develop an in-plane, rather than out-of-plane, cylindrical morphology, both in the PS matrix and at the film-air interface. As reported by Son and co-workers, 45 top coating and solvent vapor annealing can be combined to produce vertically oriented columnar PS-b-PDMS film morphologies. In order to investigate the effect of annealing solvents, a wide range of solvents including acetone, choloroform, toluene, tetrahydrofuran, and dimehylformamide were used, as shown in Figure S2. As-spun PS-b-PDMS showed a disorganized morphology (Figure S2(a)), while a treatment of solvent vapors results in in-plane (Figure S2(b)) or out-of-plane (Figure S2(c) to S2(e)) cylindrical morphologies. In our work, the optimum condition for production of the vertical cylinder morphology was found to include the use of acetone vapor to anneal the film for 2 h in a closed chamber. In addition, the influence of the PVA overlayer was also investigated (Figure 2). PS-b-PDMS films without a PVA overlayer, or with an overlayer but thermally annealed at 150 °C for 2 h, both exhibit disordered and loose-packed nanocylinders (Figures 2(a) and (b), respectively). The degree of PVA hydrolysis-40% hydrolyzed PVA (PVA-40) and 80% hydrolyzed PVA (PVA-80)-was also tested with acetone annealing for 2 h. As shown in Figure 2(c), the PVA-40-coated PS-b-PDMS film exhibits a fully vertical orientation without defects; however, dewetting was frequently observed while annealing. In contrast, the PVA-80-coated PS-b-PDMS films achieved highly oriented nanocylinders on a large scale without dewetting (Figure 2(d)). Based on the results shown in Figures 2 and S2, PVA-80 and acetone were chosen as overlayer and annealing solvent.

Since the diameter of the circular confinement corral, D, strongly affects the morphology during graphoepitaxy of BCPs, ⁴⁸ NSL templates defined in a wide range from $D \sim 5$ μm to $D \sim 150$ nm were investigated. Figure 3 and Figure S3

are representative SEM images of vertically oriented, low-defect SNC arrays formed inside circular SiO₂ corrals with different diameters. As shown in Figure 3, hexagonal close-packed arrangements of silica nanocylinders were observed inside each circular corral due to the physical confinement between PS-b-PDMS and the inner wall of the confining structure, forcing the BCPs to rearrange into uniform hierarchical nanostructures with long-range order. For comparison, more defects are observed at D = 150 nm (Figure S3), these likely arising due to the mismatch of the periodicity of the BCP cylinders and that of the NSL pattern. Furthermore, a much thinner (10–15 nm) SNC layer is observed outside the corrals. We found that it was difficult to completely avoid overcoating, even using lower concentration polymer solutions and higher spin-coating speeds. However, these nanocylinders do not contribute to the electrochemical response, as they overcoat regions not accessible to the underlying disk electrode. Overall, the highly ordered array of vertical silica nanocylinders is attributed to the combination of physical confinement provided by circular SiO₂ corrals and the well-controlled top coating and solvent vapor annealing.

3.2. Gated Ion Transport inside NEAs. NEA-based electrochemistry is not only an end to itself, but in the context of the NSL-templated PS-b-PDMS nanostructures developed here, it provides a stringent test of the integrity of the nanostructures. Ion accumulation effects are observed in 100 nm nanopore electrode arrays up to an ionic strength $\sim 10~\mu M$. However, the critical ionic strength becomes much larger when the size of the nanopore electrode is reduced; for example, $I_{\rm crit} \sim 1~{\rm mM}$ at $d_{\rm pore} \sim 10~{\rm nm}$. Thus, it is natural to seek NEAs with a high density of small diameter nanopores to exploit strong ion accumulation effects, as shown schematically in Figure 4(a). The voltammetric response was measured before (dashed line) and after (solid line) coating the ITO working electrode with SNC arrays to confirm that SNC arrays can permselectively sequester cations and reject anions. Measurements were made

with both cationic, $Ru(NH_3)_6^{3+}$, and anionic, $Fe(CN)_6^{3-}/Ru(CN)_6^{4-}$, redox species, chosen to cover a range of E^0 values at different ionic strengths, i.e., 0.5 M KCl, 1 mM KCl, and 1 μ M KCl, as shown in Figures 4(b)–(d), respectively. In the absence of silica nanochannels (bare ITO), all three cyclic voltammograms exhibit peak-shaped cathodic currents ~4 μ A, indicating the reversible redox behavior of these species (viz., dashed lines Figure 4(b)). However, modifying the ITO electrode with SNC arrays (ITO/SNC) produces diametrically opposed voltammetric responses for cationic and anionic redox species.

Furthermore, since the EDL determines the distribution and magnitude of surface charge within the SNC, it is possible to tune the ion gating properties by adjusting the electrolyte concentration, thus changing the magnitude of the Debye length, κ^{-1} . Comparison of Figures 4(b) and (c) shows that in the presence of the SNC nanochannels the currents are dramatically reduced for $Fe(CN)_6^{3-}$ and $Ru(CN)_6^{4-}$ but not for $Ru(NH_3)_6^{3+}$, a behavior consistent with the negatively charged nanochannel supporting ion accumulation of cationic $Ru(NH_3)_6^{3+}$ but repelling both $Fe(CN)_6^{3-}$ and $Ru(CN)_6^{4-}$, i.e., cation permselectivity. This gated ion transport is due to the electrostatic interaction between the inner surface of the SNC $(\zeta < 0)$ and anions. For electrolyte concentrations ≤ 1 mM, the product of the inverse Debye length and pore diameter, κd_1 approaches 1, and the EDL overlap produced by the surface charge inside the nanopores of the SNC significantly alters transport of redox species to the ITO electrode. As shown in Figures 4(c) and (d), the current obtained from $Ru(NH_3)_6^{3+}$ is changed only slightly, while the currents due to $Fe(CN)_6^{3-}$ and $Ru(CN)_6^{4-}$ are greatly suppressed, indicating that, while cations can enter the SNC nanopores at all electrolyte concentrations, anions are effectively gated. These results confirm that the electrochemical measurement can operate selectively even at modest electrolyte concentrations, e.g., 1 mM. Typically, low electrolyte concentrations are avoided due to problems such as excessive iR drop; however, previous results in our laboratory have shown that a combination of ion accumulation and ion migration effects allows NEAs to support robust faradaic currents even in the complete absence of supporting electrolyte. 17,18

The surfaces of SNC arrays are negative at neutral pH. However, it is possible to switch the surface charge from negative to positive by chemical modification. A one-step silane coupling reaction with 3-aminopropyl triethoxysilane, APTES, converts the ITO/SNC electrode assembly to an amineterminated nanochannel, ITO/SNC-NH2, which is substantially protonated near pH 7. Figure 5 shows the voltammetric responses of $Ru(NH_3)_6^{2/3+}$ and $Fe(CN)_6^{3/4-}$ on ITO/SNC (Figure 5(a)) and ITO/SNC-NH₂ (Figure 5(b)) electrodes. The ITO/SNC electrode exhibits a CV for Ru(NH₃)₆³⁺ (red) that is very similar to the CV obtained at bare ITO, whereas the peak current of Fe(CN)₆³⁻ (blue) is decreased significantly, as shown in Figure 5(a). However, the behavior is completely reversed for the ITO/SNC-NH₂ electrode. As shown in Figure 5(b), the CV of $Fe(CN)_6^{3-}$ is comparable to the response at bare ITO, while the CV of $Ru(NH_3)_6^{3+}$ produces a negligible response. The dependence of permselective voltammetric response on the magnitude of the SNC nanopore surface charge is shown in Figure S4. As the silane coupling reaction proceeds from 4 h to 9 h, the original negative nanochannel surface becomes increasingly positively charged as more amine functional groups are ligated to the surface. These observations

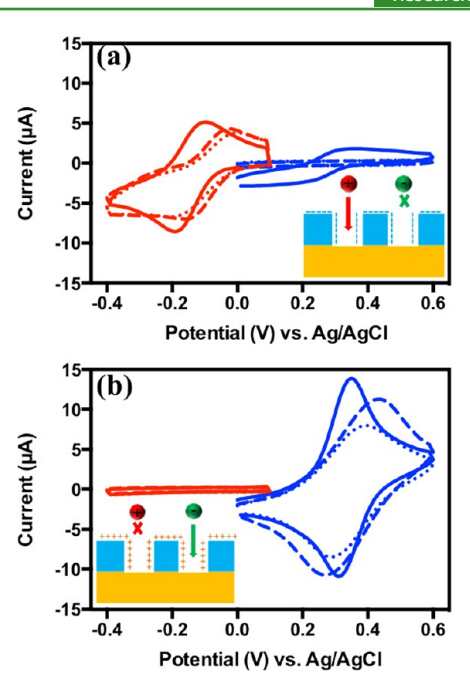


Figure 5. Cyclic voltammetry of 100 μ M Ru(NH₃) $_6^{3+}$ (red) and Fe(CN) $_6^{3-}$ (blue) in solutions of different ionic strength, [KCl] = 0.5 M (solid line), 1 mM (dashed line), 1 μ M (dotted line). (a) Voltammetry at unmodified ITO/SNC electrode. (b) Voltammetry at modified ITO/SNC-NH₂ electrode. (Insets) Schematic illustration of cation, (a), and anion, (b), permselectivity of unmodified and modified SNC nanochannels, respectively.

are consistent with permselectivity effects for cations inside positively charged nanopores and anions inside negatively charged nanopores.

The ability to lift-off and transfer the SNC array would allow the nanoscale properties built into the NSL-templated graphoepitaxial SNCs to be translated to arbitrary substrates without damaging the hierarchically organized structure. To achieve this goal, a poly(methyl methacrylate) (PMMA)assisted approach was used to transfer the SNC from ITO glass slide to other substrates.⁴⁷ As shown in Figure 6(a), the SNC array together with spun-on PMMA was released from the carrier glass slide by selectively etching the supporting ITO layer and then transferred to another ITO glass slide (other flat substrates are also suitable). The transferred SNC membrane was flat without large-scale defects (Figure 6(b)), thus preserving the originally produced hierarchical organization throughout the lift-off and transfer processes (Figure 6(c)). CVs obtained from the transferred ITO/SNC electrode were used to verify the retention of permselective electrochemical behavior at electrodes contacted with a transferred SNC NEA. Figure 6(d) shows that the shape and magnitude of CVs for $Ru(NH_3)_6^{3+}$ (red) and $Fe(CN)_6^{3-}$ (blue) remain the same on both electrodes at all electrolyte concentrations. Importantly, comparison of the behavior of 0.1 mM $Ru(NH_3)_6^{3+}$ and $Fe(CN)_6^{3-}$ shows that the permselective behavior of the ITO/ SNC electrode array at 0.5 M is largely retained after physical transfer of the ITO/SNC nanostructure to a different substrate.

4. CONCLUSIONS

In summary, the results reported here demonstrate that the novel combination of NSL-templated graphoepitaxy of PS-b-PDMS followed by PVA overcoating, solvent annealing, and O₂-plasma treatment produces highly ordered silica nano-

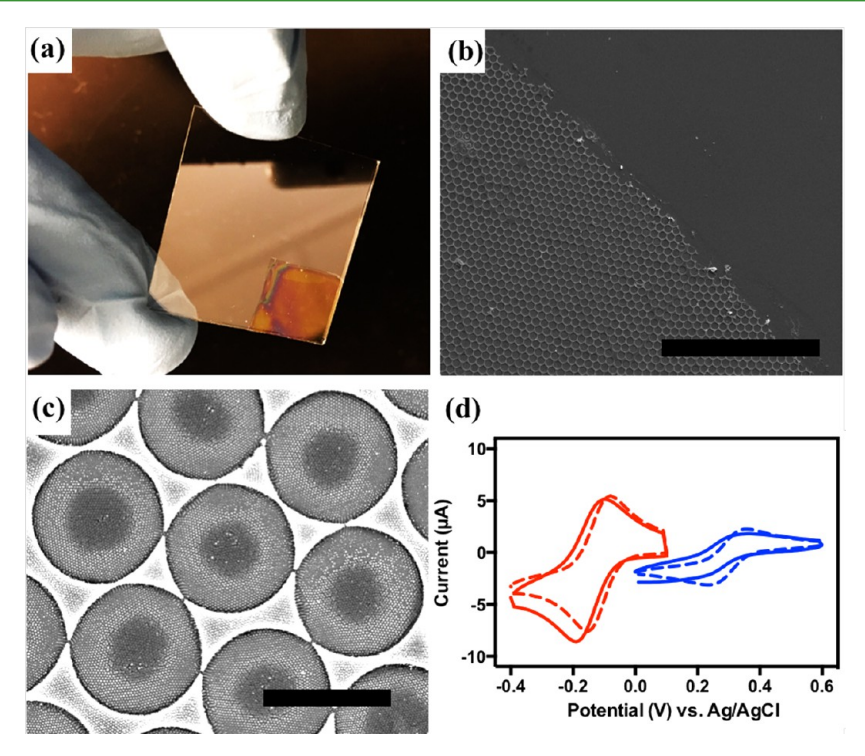


Figure 6. (a) Photo of an SNC membrane intentionally delaminated from the ITO substrate by lift-off in DI water and transferred to a separate ITO/glass substrate. (b) and (c) are SEM images of transferred SNC membrane at low and high magnification, respectively. Scale bars: 40 and 2 μ m in (b) and (c), respectively. (d) Cyclic voltammetry at original as-prepared (solid line) and transferred (dashed line) ITO/SNC electrodes with 0.1 mM Ru(NH₃)₆³⁺ (red) and Fe(CN)₆³⁻ (black) in 0.5 M KCl electrolyte.

channels with areal densities approaching 1000 elements μm^{-2} and aspect ratios >5:1 on a large scale. The resulting ultrahigh density SNC arrays are competent to serve as ion gates to discriminate between cationic and anionic species, due to the permselective character of the SNC nanochannels. This surface charge-dominated behavior was demonstrated by suppression of current from anionic redox species, while almost no change of current was observed for cationic redox species. Furthermore, the polarity of the permselective behavior can be flipped by chemically modifying the SNC nanochannel surfaces with positively charged amine groups, i.e., screening positively charged species and accumulating negatively charged redox analytes. Finally, the massively parallel fabrication strategy produces high density nanoscale SNC arrays over large scales, which can subsequently be transferred to another substrate without damaging the molecular sieving or ion gating properties. This proof-of-concept sets the stage for potential applications in preconcentration of target molecules and improved electrochemical selectivity for electrode materials not capable of supporting the SNC fabrication process directly.

ASSOCIATED CONTENT

S Supporting Information

The Supporting Information is available free of charge on the ACS Publications website at DOI: 10.1021/acsami.7b06794.

SEM images of the effect of different solvents on solvent annealing, the pattern size on the directed self-assembly of PS-bPDMS, and electrochemical results showing the dependence of chemical modification on the silica nanochannel arrays (PDF)

AUTHOR INFORMATION

Corresponding Author

*P.W. Bohn. E-mail: pbohn@nd.edu.

ORCID (

Kaiyu Fu: 0000-0002-7899-0388 Paul W. Bohn: 0000-0001-9052-0349

Notes

The authors declare no competing financial interest.

■ ACKNOWLEDGMENTS

This work was supported by the National Science Foundation grant 1404744. We gratefully acknowledge C. Ma for valuable discussions and Notre Dame Nanofabrication Facility and Integrated Imaging Facility for providing fabrication and structural characterization of the devices studied here.

■ REFERENCES

- (1) Ozbay, E. Plasmonics: Merging photonics and electronics at nanoscale dimensions. *Science* **2006**, *311*, 189–193.
- (2) Jain, P. K.; Huang, X.; El-Sayed, I. H.; El-Sayed, M. A. Noble Metals on the Nanoscale: Optical and Photothermal Properties and Some Applications in Imaging, Sensing, Biology, and Medicine. *Acc. Chem. Res.* **2008**, *41*, 1578–1586.
- (3) Murray, R. W. Nanoelectrochemistry: Metal Nanoparticles, Nanoelectrodes, and Nanopores. *Chem. Rev.* **2008**, *108*, 2688–2720.
- (4) Arrigan, D. W. M. Nanoelectrodes, nanoelectrode arrays and their applications. *Analyst* **2004**, *129*, 1157–1165.
- (5) Bae, J. H.; Han, J.-H.; Chung, T. D. Electrochemistry at nanoporous interfaces: new opportunity for electrocatalysis. *Phys. Chem. Chem. Phys.* **2012**, *14*, 448–463.
- (6) Dawson, K.; O'Riordan, A. Electroanalysis at the Nanoscale. *Annu. Rev. Anal. Chem.* **2014**, *7*, 163–181.
- (7) LaFratta, C. N.; Walt, D. R. Very High Density Sensing Arrays. *Chem. Rev.* **2008**, *108*, 614–637.

- (8) Hou, X.; Guo, W.; Jiang, L. Biomimetic smart nanopores and nanochannels. *Chem. Soc. Rev.* **2011**, *40*, 2385–2401.
- (9) Dickinson, E. J. F.; Compton, R. G. Diffuse Double Layer at Nanoelectrodes. *J. Phys. Chem. C* **2009**, *113*, 17585–17589.
- (10) Piruska, A.; Gong, M.; Sweedler, J. V.; Bohn, P. W. Nanofluidics in chemical analysis. *Chem. Soc. Rev.* **2010**, *39*, 1060–1072.
- (11) Xiong, J.; Chen, Q.; Edwards, M. A.; White, H. S. Ion Transport within High Electric Fields in Nanogap Electrochemical Cells. *ACS Nano* **2015**, *9*, 8520–8529.
- (12) Stein, D.; Kruithof, M.; Dekker, C. Surface-Charge-Governed Ion Transport in Nanofluidic Channels. *Phys. Rev. Lett.* **2004**, 93, 035901.
- (13) Karnik, R.; Fan, R.; Yue, M.; Li, D.; Yang, P.; Majumdar, A. Electrostatic Control of Ions and Molecules in Nanofluidic Transistors. *Nano Lett.* **2005**, *5*, 943–948.
- (14) Krapf, D.; Quinn, B. M.; Wu, M.-Y.; Zandbergen, H. W.; Dekker, C.; Lemay, S. G. Experimental Observation of Nonlinear Ionic Transport at the Nanometer Scale. *Nano Lett.* **2006**, *6*, 2531–2535.
- (15) Oja, S. M.; Wood, M.; Zhang, B. Nanoscale Electrochemistry. *Anal. Chem.* **2013**, *85*, 473–486.
- (16) Oja, S. M.; Fan, Y.; Armstrong, C. M.; Defnet, P.; Zhang, B. Nanoscale Electrochemistry Revisited. *Anal. Chem.* **2016**, *88*, 414–430
- (17) Ma, C.; Xu, W.; Wichert, W. R. A.; Bohn, P. W. Ion Accumulation and Migration Effects on Redox Cycling in Nanopore Electrode Arrays at Low Ionic Strength. ACS Nano 2016, 10, 3658–3664.
- (18) Fu, K.; Han, D.; Ma, C.; Bohn, P. W. Ion selective redox cycling in zero-dimensional nanopore electrode arrays at low ionic strength. *Nanoscale* **2017**, *9*, 5164–5171.
- (19) Sandison, M. E.; Cooper, J. M. Nanofabrication of electrode arrays by electron-beam and nanoimprint lithographies. *Lab Chip* **2006**, *6*, 1020–1025.
- (20) Bai, J.; Wang, D.; Nam, S.-w.; Peng, H.; Bruce, R.; Gignac, L.; Brink, M.; Kratschmer, E.; Rossnagel, S.; Waggoner, P.; Reuter, K.; Wang, C.; Astier, Y.; Balagurusamy, V.; Luan, B.; Kwark, Y.; Joseph, E.; Guillorn, M.; Polonsky, S.; Royyuru, A.; Papa Rao, S.; Stolovitzky, G. Fabrication of sub-20 nm nanopore arrays in membranes with embedded metal electrodes at wafer scales. *Nanoscale* **2014**, *6*, 8900–8906.
- (21) Huske, M.; Stockmann, R.; Offenhausser, A.; Wolfrum, B. Redox cycling in nanoporous electrochemical devices. *Nanoscale* **2014**, *6*, 589–598.
- (22) Lanyon, Y. H.; De Marzi, G.; Watson, Y. E.; Quinn, A. J.; Gleeson, J. P.; Redmond, G.; Arrigan, D. W. M. Fabrication of Nanopore Array Electrodes by Focused Ion Beam Milling. *Anal. Chem.* **2007**, *79*, 3048–3055.
- (23) Han, D.; Zaino, L. P.; Fu, K.; Bohn, P. W. Redox Cycling in Nanopore-Confined Recessed Dual-Ring Electrode Arrays. *J. Phys. Chem. C* **2016**, *120*, 20634–20641.
- (24) Henzie, J.; Barton, J. E.; Stender, C. L.; Odom, T. W. Large-Area Nanoscale Patterning: Chemistry Meets Fabrication. *Acc. Chem. Res.* **2006**, *39*, 249–257.
- (25) Bang, J.; Jeong, U.; Ryu, D. Y.; Russell, T. P.; Hawker, C. J. Block Copolymer Nanolithography: Translation of Molecular Level Control to Nanoscale Patterns. *Adv. Mater.* **2009**, *21*, 4769–4792.
- (26) Kim, H.-C.; Park, S.-M.; Hinsberg, W. D. Block Copolymer Based Nanostructures: Materials, Processes, and Applications to Electronics. *Chem. Rev.* **2010**, *110*, 146–177.
- (27) Koo, K.; Ahn, H.; Kim, S.-W.; Ryu, D. Y.; Russell, T. P. Directed self-assembly of block copolymers in the extreme: guiding microdomains from the small to the large. *Soft Matter* **2013**, *9*, 9059–9071.
- (28) Jung, Y. S.; Ross, C. A. Orientation-Controlled Self-Assembled Nanolithography Using a Polystyrene–Polydimethylsiloxane Block Copolymer. *Nano Lett.* **2007**, *7*, 2046–2050.
- (29) Ruiz, R.; Kang, H.; Detcheverry, F. A.; Dobisz, E.; Kercher, D. S.; Albrecht, T. R.; de Pablo, J. J.; Nealey, P. F. Density Multiplication and Improved Lithography by Directed Block Copolymer Assembly. *Science* **2008**, *321*, 936–939.

- (30) Xu, J.; Park, S.; Wang, S.; Russell, T. P.; Ocko, B. M.; Checco, A. Directed Self-Assembly of Block Copolymers on Two-Dimensional Chemical Patterns Fabricated by Electro-Oxidation Nanolithography. *Adv. Mater.* **2010**, *22*, 2268–2272.
- (31) Xiang, H.; Shin, K.; Kim, T.; Moon, S. I.; McCarthy, T. J.; Russell, T. P. Block Copolymers under Cylindrical Confinement. *Macromolecules* **2004**, *37*, 5660–5664.
- (32) Stoykovich, M. P.; Müller, M.; Kim, S. O.; Solak, H. H.; Edwards, E. W.; de Pablo, J. J.; Nealey, P. F. Directed Assembly of Block Copolymer Blends into Nonregular Device-Oriented Structures. *Science* 2005, 308, 1442–1446.
- (33) Stein, G. E.; Kramer, E. J.; Li, X.; Wang, J. Single-Crystal Diffraction from Two-Dimensional Block Copolymer Arrays. *Phys. Rev. Lett.* **2007**, *98*, 086101.
- (34) Yi, H.; Bao, X.-Y.; Zhang, J.; Bencher, C.; Chang, L.-W.; Chen, X.; Tiberio, R.; Conway, J.; Dai, H.; Chen, Y.; Mitra, S.; Wong, H. S. P. Flexible Control of Block Copolymer Directed Self-Assembly using Small, Topographical Templates: Potential Lithography Solution for Integrated Circuit Contact Hole Patterning. *Adv. Mater.* **2012**, *24*, 3107–3114.
- (35) Gopinadhan, M.; Deshmukh, P.; Choo, Y.; Majewski, P. W.; Bakajin, O.; Elimelech, M.; Kasi, R. M.; Osuji, C. O. Thermally Switchable Aligned Nanopores by Magnetic-Field Directed Self-Assembly of Block Copolymers. *Adv. Mater.* **2014**, *26*, 5148–5154.
- (36) Kathrein, C. C.; Bai, W.; Currivan-Incorvia, J. A.; Liontos, G.; Ntetsikas, K.; Avgeropoulos, A.; Böker, A.; Tsarkova, L.; Ross, C. A. Combining Graphoepitaxy and Electric Fields toward Uniaxial Alignment of Solvent-Annealed Polystyrene-b-Poly-(dimethylsiloxane) Block Copolymers. *Chem. Mater.* **2015**, 27, 6890–6898.
- (37) Zschech, D.; Kim, D. H.; Milenin, A. P.; Scholz, R.; Hillebrand, R.; Hawker, C. J.; Russell, T. P.; Steinhart, M.; Gösele, U. Ordered Arrays of (100) -Oriented Silicon Nanorods by CMOS-Compatible Block Copolymer Lithography. *Nano Lett.* **2007**, *7*, 1516–1520.
- (38) Jung, Y. S.; Ross, C. A. Well-Ordered Thin-Film Nanopore Arrays Formed Using a Block-Copolymer Template. *Small* **2009**, *5*, 1654–1659.
- (39) Li, T.; Wang, Z.; Schulte, L.; Ndoni, S. Substrate tolerant direct block copolymer nanolithography. *Nanoscale* **2016**, *8*, 136–140.
- (40) Han, E.; Stuen, K. O.; Leolukman, M.; Liu, C.-C.; Nealey, P. F.; Gopalan, P. Perpendicular Orientation of Domains in Cylinder-Forming Block Copolymer Thick Films by Controlled Interfacial Interactions. *Macromolecules* **2009**, 42, 4896–4901.
- (41) Son, J. G.; Gotrik, K. W.; Ross, C. A. High-Aspect-Ratio Perpendicular Orientation of PS-b-PDMS Thin Films under Solvent Annealing. *ACS Macro Lett.* **2012**, *1*, 1279–1284.
- (42) Yin, J.; Yao, X.; Liou, J.-Y.; Sun, W.; Sun, Y.-S.; Wang, Y. Membranes with Highly Ordered Straight Nanopores by Selective Swelling of Fast Perpendicularly Aligned Block Copolymers. *ACS Nano* **2013**, *7*, 9961–9974.
- (43) Gu, W.; Hong, S. W.; Russell, T. P. Orienting Block Copolymer Microdomains with Block Copolymer Brushes. *ACS Nano* **2012**, *6*, 10250–10257.
- (44) Bates, C. M.; Seshimo, T.; Maher, M. J.; Durand, W. J.; Cushen, J. D.; Dean, L. M.; Blachut, G.; Ellison, C. J.; Willson, C. G. Polarity-Switching Top Coats Enable Orientation of Sub–10-nm Block Copolymer Domains. *Science* **2012**, 338, 775–779.
- (45) Kim, E.; Kim, W.; Lee, K. H.; Ross, C. A.; Son, J. G. A Top Coat with Solvent Annealing Enables Perpendicular Orientation of Sub-10 nm Microdomains in Si-Containing Block Copolymer Thin Films. *Adv. Funct. Mater.* **2014**, *24*, 6981–6988.
- (46) Fu, K.; Han, D.; Ma, C.; Bohn, P. W. Electrochemistry at single molecule occupancy in nanopore-confined recessed ring-disk electrode arrays. *Faraday Discuss.* **2016**, *193*, 51–64.
- (47) Lin, X.; Yang, Q.; Ding, L.; Su, B. Ultrathin Silica Membranes with Highly Ordered and Perpendicular Nanochannels for Precise and Fast Molecular Separation. *ACS Nano* **2015**, *9*, 11266–11277.
- (48) Pitet, L. M.; Alexander-Moonen, E.; Peeters, E.; Druzhinina, T. S.; Wuister, S. F.; Lynd, N. A.; Meijer, E. W. Probing the Effect of

Molecular Nonuniformity in Directed Self-Assembly of Diblock Copolymers in Nanoconfined Space. *ACS Nano* **2015**, *9*, 9594–9602.